LAWRENCE
LIVERMORE
NATIONAL
LABORATORY

LLNL-PROC-870281

TATB Thermal Decomposition: An Improved Kinetic Model for Explosive Safety Analysis

J. S. Moore, A. Racoveanu, K. D. Morrison, A. K. Burnham, B. Koroglu, G. L. Klunder, J. G. Reynolds

October 7, 2024

2024 International Explosives Conference
Edinburgh, United Kingdom
June 18, 2024 through June 21, 2024

Disclaimer

TATB Thermal Decomposition: An Improved Kinetic Model for Explosive Safety Analysis

Keith R. Coffee,[a*] Jason S. Moore,[a] Ana Racoveanu,[b] Keith D. Morrison,[a] Alan K. Burnham,[c] Batikan Koroglu,[a] Gregory L. Klunder,[a] & John G. Reynolds[a]

DOI: 10.1039/ISBN-00xxx [DO NOT ALTER/DELETE THIS TEXT]

TATB (1,3,5-triamino-2,4,6-trinitro benzene) and polymeric formulations, are widely used energetic material applications. LLNL, as with many other laboratories, evaluates these materials to assure safe handling. This is a summary of the process of developing a new, expanded thermal decomposition model to address the behavior of TATB and formulations exposed to abnormal thermal environments. Ultimately, this model is used to assist determining the safety aspects of TATB, or any other explosive, when thermally compromised. This work is the culmination of global behavior and molecular characterization studies to increase the accuracy of the reaction sequences in the model. This report will review the science developed leading to the model, culminating with the model.

1 Introduction

TATB is the basis of all the insensitive high explosives (IHEs) of today. The compound itself has been around since the later 1800s, but it was not until the second half of the 1900s that it was recognized as an explosive. Figure 1 left shows the molecule itself, having the carbon configured into a benzene ring, with alternating amino and nitro substitutions around the ring. It is fully substituted, with all positions on the benzene ring occupied, and these functional groups available for secondary interactions of hydrogen bonding, both intra and intermolecular. Figure 1 middle shows distorted planar array of TATB molecules linked by in plane hydrogen bonds. These hydrogen bonds extend in three dimensions, which maintains the somewhat distorted structure. Figure 1 right shows how these planes come together as layers forming a tertiary structure.[1-3]

[Insert Figure 1 here]

TATB is considered an insensitive explosive because of the lack of response to external stimuli, such as impact, friction, spark and heating. To put it in perspective, the decomposition temperatures are easily 100 °C more stable than PETN or HMX. Because of the wide use of TATB, its thermal stability is an important issue. The impetus of this research is to understand what happens to TATB when heated or exposed to an abnormal thermal environment, whether purposely or not. The development of a thermal decomposition model is the major driving force because it is related to safety.

[Insert Figure 2 here]

Figure 2 shows the results of laboratory experiments designed to explore the effects of thermal exposure at various severities.[4] Under mild conditions,[5] the top of Figure 2, TATB can go from discoloration (200 °C/6 h-image) to gradually attrition (250 °C/6 h-image). In more severe conditions[6] (SSVCT images), the heating can lead to char formation and enough gas production to open confinement. If heated under severe conditions[7] (STEX images), the reactor will rupture, scattering the char and unreacted TATB.

The model was built from earlier work proposing a reduced reaction network.[8] It uses only explicit chemical reactions. The data were used to fit rate parameters for proposed reaction schemes in a MATLAB thermos-chemical computational model. These parameterizations were carried out utilizing a genetic algorithm optimized on LLNL's high performance computing clusters, which enabled significant parallelization including a multi-step decomposition model, identification of likely autocatalytic gas-phase species, predictive sensitization and effects of confinement.[9]

Five key areas of characterization research helped in the development of the model:

- Heat and mass balance to develop global kinetic models (Differential scanning calorimetry and thermogravimetric (DSC-TGA) analyses)
- Pyrolysis decomposition with on-line analyses to detect gaseous decomposition compounds (pyrolysis-chromatography-mass spectrometry (py-GC-MS))
- High performance chromatography to separate decomposition compounds in the solid phase with molecular identification by mass spectrometry (DMSO extraction with HPLC-DAD/MS)
- Synthetic substitution of spectroscopic probes into TATB structure (isotopic substitution, ^{15}N, ^{2}H, ^{13}C, ^{18}O)
- Characterization by miscellaneous spectroscopic methods of thermal products (SS NMR, FTIR, hot stage microscope with IR, XPS, TEM, PXRD)

Characterization on both the global-level and molecular-level was key to development of the model. The global experimentation gave us the overall behaviour and the molecular level delineated the specific reaction chemistry occurring.

This report is derived directly from the presentation (Session 3: AI & Machine Learning) at the 2024 International Explosives Conference in Edinburgh, Scotland, and summarizes the development of a new and improved thermal decomposition model for TATB.[10] More complete details of the experiments, data, and model developments are given in the references within.

2 Development of Model

2.1 Background in TATB Thermal Decomposition Models

Figure 3 summarizes of the thermal decomposition models for TATB, starting around 1950. The challenge for this type of chemistry is how to evaluate how solid-state materials begin to react or decompose. The first models had single-step reactions of reactants converting to products, such as the Prout-Tompkins.[11] As models progressed in complexity

[a] *Lawrence Livermore National Laboratory, Livermore CA, USA, +1 925 423 2292; E-mail: coffee3@llnl.gov*
b. NorthWind Services, LLC, Livermore CA USA
c. Stratify//MH Chew Associates, Livermore CA USA

due to more experimental input, they have increased in steps of reactions, both parallel[12] and in series.[13] An important addition was earlier in this century specifically calling out the involvement water in the first step.[14] This is relevant when considering at the same time, many studies observed the formation of furazans as a first thermal reaction steps and by extension, the condensation reaction forms water.

[Insert Figure 3 here]

2.2 TATB Global Thermal Profiles

Figure 4 shows the results of the differential scanning calorimetry (DSC) examination of TATB. These results were generated by measuring heat flow and mass loss on analytical equipment (simultaneous DSC and thermogravimetric analyses, TGA). The profiles are from multiple heating rates (0.5, 1.0, 5.0, & 10.0 °C/min). Although the range of temperatures of response varies depending upon the heating rate, the overall profile shape remains reasonably consistent. The profiles can be resolved into two overlapping exotherms with the leading-edge shoulder overlapping with a sharp major exotherm. These represent two global reactions, and with the proper examination by DSC and TGA, the global kinetics can be derived. The application of kinetic analysis using different constant heating rate profiles and a typical kinetic analyses method (in this case Kissinger's method) the activation energy parameters can be derived.[15]

[Insert Figure 4 here]

Earlier work using mass spectrometry (MS) demonstrated the evolving gases resulting from thermal decomposition can be different indicating the precursors to these two global reactions are not the same.[16] Several studies have verified the composition of the volatile species evolving change with decomposition temperature.

2.3 Compound Evolution during DSC

Recent efforts have analysed the gaseous effluent during thermal decomposition in more detail. Utilizing MS, the molecular composition of volatile compounds can be measured. Figure 5 shows two examples such evolving compounds. The left side shows compounds evolving from a large-scale cook-off.[17] The experiment was heated at 29 °C/min heating rate. The evolution shows some gases evolve sooner than others and before the main event which starts around 236 °C. Figure 5 right side shows a simultaneous DSC TGA coupled to MS (SDT-MS) experiment monitoring light gases at a 1 °C/min heating rate.[18] This experiment also correlates the gas evolution with the exotherms, as seen in Figure 4. Again, there are two sets of evolving gases correlating with the two global reactions. It is notable that CO_2 and H_2O are early evolving and stand out.

[Insert Figure 5 here]

2.4 Compounds Evolving during Pyrolysis Mass Spectrometry

Further identification of the compounds evolving during thermal degradation comes from flash pyrolysis of TATB with MS detection in isothermally heated samples.[19] Figure 6 shows an example of the evolution profiles at 330 °C over a period of 70 min. The top profile is the total ion current (TIC) and below are the behaviors of selected individual molecules during heating. The bimodal distribution seen in the constant heating rate experiments, as in Figures 4 & 5, is not pronounced in the TIC profile. However, CO_2 and NO_2, and H_2O evolve early (the dashed red line) while all the materials evolve later (the dashed purple line). The CO_2 comes from the oxidation of the TATB ring. This has been proven by decomposing ^{13}C and ^{18}O isotopic substituted TATB compounds under the same

conditions. The role of NO_2 also appears to be an early forming reactant and offers a new pathway for TATB decomposition.

[Insert Figure 6 here]

2.5 Decomposition Pathways of TATB—Global and Molecular

Establishing the relationship of the overall reaction behavior with the molecular composition yields insight into molecular origins of the two global overlapping exotherms. Figures 5 & 6 indicate the precursor compounds to the evolved species for the two exotherms are possibly different. TATB was isothermally treated in a DSC-TGA for different reaction times producing a suite of samples. The heat flow and weight loss observed and sample masses before and after were measured to provide a pseudo-mass balance.[20] The molecular composition at each reaction time was also measured by extraction of the soluble portion followed by compositional analyses.[21,22] Linking the molecular profile with the mass distribution helps correlate global and molecular reactions. Figure 7 left side shows the residue composition divided into soluble (DMSO extractable components), insoluble (DMSO insoluble residue) portion, volatiles (mass difference before and after reaction), and the TATB concentration (by analyses of the extractable portion). These results were obtained from small samples painfully handled to give a mass balance and analytically accurate composition. TATB decreases in a sigmoidal behavior and is no longer present at 65 min. The solid and volatiles gradually grow in concentration. However, at 65 min, there appears to be a disruption as the TATB concentration disappears (as measured by extraction). the volatile and solid content increases.

[Insert Figure 7 here]

The same samples were extracted with DMSO, and the composition determined by column separation followed mass spectrometric identification.[21] TATB was quantitated by methods recently developed.[22] At 65 min, there is a real change in the composition, which is when the TATB becomes exhausted. However, volatiles and char continued to be produced. Notice the sigmodal behavior of TATB decomposition. Figure 7 right side shows some of the other species that were found in the soluble extract by HPLC/optical/MS detection developed in this project. For the other species T4A and HO-TATB, which were found in the starting material, monotonically decrease with time. Reaction products related to TATB, the furazans (F_1, F_2, HO-F_2) and mono-nitroso-TATB (MN-TATB) obviously were formed then destroyed during the heating. These also had the concentration drop-off at 65 min. These results elucidate the benzo-furazan decomposition pathways.

3 Chemical Reaction Pathways

The above provide examples of global and chemical characterization of the thermal decomposition pathways of TATB. Through molecular characterization techniques developed for this project, these results have produced two overall pathways for thermal decomposition—furazan and oxidation by NO_2. Figure 8 shows the general types of reactions.

[Insert Figure 8 here]

The furazan pathway on the left side has been known for several decades and has been well studied.[6,16,17,23,24] This current work has added some more decomposition products and conditions.[19] The other pathway on the right side, which has been recognized for many explosives, but not for TATB, is the oxidation mechanism.[18] NO_2 is involved, but it is not clear whether it is the active species or reacts producing active species. However, this has not been proposed or verified for TATB previously. These two major characterization

schemes have greatly expanded the model to be more inclusive to chemistry and more accurate for prediction.

[Insert Figure 9 here]

Figure 9 shows more details of these chemical reactions and the inter relationships among the chemical species, and includes some of the species from the characterization work.[25] The NO_2, a fierce oxidant, can come from various species. Also, this shows how the ring unzips producing species like C_2N_2 and HNCO (bottom right).

4 Improved Thermal Decomposition Model

4.1 Model Description

Figure 10 shows the improved thermal model, expanding the number and complexity of the reactions compared to the earlier models cited above.[9] This model includes more detailed analyses of the intermediates and products both on the bulk and molecular level. It is important to point out the roles of the intermediates molecularly identified for the first time. Chemical species, such as NO_2 and early forming CO_2, are recognized as critical components. Briefly, the TATB reacts to give mono-benzo-furazan (F_1). The F_1 continues to react forming more condensed products called solid intermediates or SIs. These are a variety of compounds molecularly identified and some examples are discussed in preceding sections. Also, TATB loses and reacts with early forming NO_2, something not delineated until now, which causes oxidation reactions. NO_2 can be produced by scission from other species as well, such as dibenzo-furazan (F_2) . See Figure 9 for other examples. Many light gases are formed, such as HNCO, C_2N_2 etc., with the final products being a carbon-nitride residue (CN residue) and several non-condensable gases.

[Insert Figure 10 here]

Figure 11 shows the reaction network.[9] A genetic algorithm was used to parameters orthogonalized E_a and k_0 for five reactions. The first reaction is the water equilibrium step. Direct formation of mono-benzo-furazan leads to water formation as well. Mono-benzo-furazan decomposes to solid intermediates which include other furazans, as indicated in Figure 9. TATB also reacts with some form of NO_2. F_1 also reacts with some form of NO_2. The solid intermediates react giving char residue. The is a solid residue reaction that has the C_2N_2 term dependence.

[Insert Figure 11 here]

4.2 Examples of simulations from the model compared to measurements

The model was developed with a variety of data including one dimensional time to explosion (PODTX), DSC, TGA, burst time, etc.[9,26] Figure 12 left side shows the comparison of the modeled PODTX for LX-17 (92.5 wt. % TATB and 7.5 wt. % Kel-F) indicating times to explosion at four different densities showing the effect of gas pressure on the rate of autocatalysis. The insets are the temperature gradients in the residual material at the end of the simulations. Heat transfer varies depending upon temperature. Figure 12 right side shows a comparison of the DSC data and simulation at 10 °C/min heating rate. The overlapping exotherms shown in Figures 4 & 5 are better seen in simulations under isothermal decomposition conditions. More detailed comparisons, such as TGA, pressure profiles in PODTX, and explosion/burst times are provided elsewhere.[9,26]

[Insert Figure 12 here]

5 Conclusions

A new, improved thermal decomposition model for TATB and related materials has been developed which includes improvements in number and types of reactions. Comparison of simulations with thermal decomposition experimental data show excellent agreement. Global reaction and molecular characterization studies provided new information relevant to development of detailed features of the model.

- Global reaction network must include at least two autocatalytic reactions, either in parallel or series, and at least one must have an explicit initiation reaction having a low activation energy
- Molecular characterization shows two predominant decomposition reactions—furazan decomposition and oxidation facilitated by NO_2
- Ring carbon oxidation occurs early in competition of furazan condensation reactions

This work addresses the need for an improved safety understanding when dealing with TATB and formulations exposed to abnormal thermal environments.

6 Acknowledgement

This work was performed under the auspices of the U.S. Department of Energy by Lawrence Livermore National Laboratory under Contract DE-AC52-07NA27344**.** LLNL-CONF-###### (1104967).

7 References

1 H. H. Cady, A. C. Larson, *Acta Crystallogr*. 1965, **18,** 485–496. doi: 10.1107/S0365110X6500107X;

2 Z. Chua, C. G. Gianopoulos, B. Zarychta, E. A. Zhurova, V. V. Zhurov, A. A. Pinkerton, Cryst. Growth Des. 2017, **17**, 5200−5207. doi: 10.1021/acs.cgd.7b00674.

3 H. E. Mason, C. A. Colla, A. Racoveanu, K. R. Coffee, A. F. Panasci-Nott, E.M. Kahl, J.G. Reynolds, *J. Phys. Chem. C* 2022, **126**, 18802–18812, DOI: 10.1021/acs.jpcc.2c03405.

4 J. G. Reynolds, A. Racoveanu, A. K. Burnham, J. S. Moore, K. R. Coffee, A. F. Panasci-Nott, K. D. Morrison, B. Koroglu, G. L. Klunder, C. A. Colla, J. Lee, H. E. Mason, J. D. Van Horn, E. M. Kahl, APS SCCM Meeting, Chicago, IL 6.19.22-6.23.23, LLNL-PRES-850235.

5 P. C. Hsu, G. Hust, W. M. Howard, & J. L. Maienschein, *Proceedings of the 14th International Detonation Symposium*, 984-990, 2010.

6 J. G. Reynolds, N. K. Muetterties, A. J. Nelson, H. E. Mason, J. S. Moore, K. R. Coffee, E. M. Kahl, *Propellants Explos. Pyrotech.* 2021, **46,** 1–15, DOI: prep.202100034.

7 J. F. Wardell, J. L. Maienschein, *Proceedings of the 12th International Detonation Symposium*, 2002, 384-393, Office of Naval Research, ONR-333-05-2, San Diego, CA.

8 J. S. Moore, M. A. McClelland, P. C. Hsu, G. F. Ellsworth, E. M. Kahl, H. K. Springer, *Proceedings of the 16th International Detonation Symposium*, Cambridge, MD, **2018**, pp. 936–945.

9 J. S. Moore, K. D. Morrison, A. K. Burnham, A. Racoveanu, J. G. Reynolds, B. Koroglu, K. R. Coffee, G. L. Klunder, *Propellants, Explos., Pyrotech*. 2023, 48, e202300237. https://doi.org/10.1002/prep.202300237.

10 K. R. Coffee, J. S. Moore, A. Racoveanu, K. D. Morrison, A. K. Burnham, B. Koroglu, G. L. Klunder, & J. G. Reynolds, TATB thermal decomposition: An improved kinetic model for explosive safety analysis, International Explosives Conference, Edinburgh, Scotland, Lawrence Livermore National Laboratory report, LLNL-PRES-863995 (1074727), 6.19.24.

11 E. G. Prout & F. C. Tompkins, *Trans. Farady Soc.*, 1944, **40**, 488-498, 1944.

12 R. R. McGuire & C. M. Tarver, *Proceedings of the 7th International Detonation Symposium*, Naval Surface Weapons Center NSWC MP 82–334, Annapolis, MD, June 10–19, **1981**, 56–64

13 C. M. Tarver, S. K. Chidester, & A. L. Nichols, *J. Phys. Chem*., 1996, **100**, 5794-5799.

14 M. L. Hobbs & M. J. Kaneshige, *J. Chem. Phys*., 2014, **140**, 124203.

15 A. K. Burnham, K. R. Coffee, G. L. Klunder, A. F. Panasci-Nott, & J. G. Reynolds, LLNL report JRNL-848399. *Propellants, Explos., Pyrotech.* 2023, 48, e202300121. https://doi.org/10.1002/prep.202300121.

16 T. A. Land, W. J. Siekhaus, M. F. Foltz, R. Behrens Jr., *Proceedings of the 10th Symposium (International) on Detonation*, Boston, MA, **1983**, 181–189.

17 B. J. Yancey, N. K. Muetterties, E. M. Kahl, E. A. Glascoe, J. G. Reynolds, *Proceedings of the 16th Symposium (Inter- national) on Detonation*, **2018**, ONR-43-5762-19, 1664–1675.

18 K. D. Morrison, A. Racoveanu, J. S. Moore, A. K. Burnham, B. Koroglu, K. R. Coffee, A. F. Panasci-Nott, G. L. Klunder, B. A. Steele, M. A. McClelland, J. G. Reynolds, LLNL report, JRNL-852686, *Sci. Rep.* **13**, 21256 (2023). https://doi.org/10.1038/s41598-023-47952-6

19 K. D. Morrison, J. S. Moore, K. R. Coffee, B. Koroglu, A. K. Burnham, J. G. Reynolds, LLNL Report JRNL-853782, *Propellants, Explos., Pyrotech*. 2023 48, e202300268. https://doi.org/10.1002/prep.202300268.

20 A. K. Burnham, K. R. Coffee, G. L. Klunder, A. F. Panasci-Nott, & J. G. Reynolds, LLNL report JRNL-848399. *Propellants, Explos., Pyrotech.* 2023, 48, e202300121. https://doi.org/10.1002/prep.202300121;

21 K. R. Coffee, A, F. Panasci-Nott, J. A. Olivas, J. Selinsky, K. D. Morrison, A. K. Burnham, G. L. Klunder, J. G. Reynolds, *Propellants, Explos., Pyrotech.* **2023**, DOI: 10.1002/ prep.202300176.

22 K. R. Coffee, A. F. Panasci-Nott, B. J. Stewart, J. A. Olivas, A. M. Williams, J. G. Reynolds, *Propellants Explos. Pyrotech.* **2022**, *47*, e202100224, DOI: 10.1002/prep.202100224.

23 J. Sharma, W. L. Garrett, F. J. Owens, V. L. Vogel, *J. Phys. Chem.* **1982**, *86*, 1657–1661. doi: 10.1021/ j100206a034.

24 R. Belmas, A. Bry, C. David, L. Gautier, A. Keromnes, D. Poul- lain, G. Thevenot, C. Le Gallic, J. Chenault, G. Guillaumet, *Propellants Explos. Pyrotech.* **2004**, *29*, 282–286, DOI: 10.1002/prep.200400059.

25 J. S. Moore, K. D. Morrison, A. K. Burnham, A. Racoveanu, B. Koroglu, K. R. Coffee, A. F. Panasci-Nott, G. L. Klunder, B. A. Steele, M. A. McClelland, J. D. Van Horn, & J. G. Reynolds, Lawrence Livermore National Laboratory Report, LLNL-TR-850231, DOPSR 23-S-2313, 2023.

26 J. S. Moore, A. K. Burnham, K. D. Morrison, A. Racoveanu, K. R. Coffee, B. Koroglu, G. L. Klunder, J. G. Reynolds, APS Shock Compression of Condensed Matter Conference, Chicago, IL 6.20.23, Lawrence Livermore National Laborastory Report, LLNL-PRES-849784, 2023.

Figures

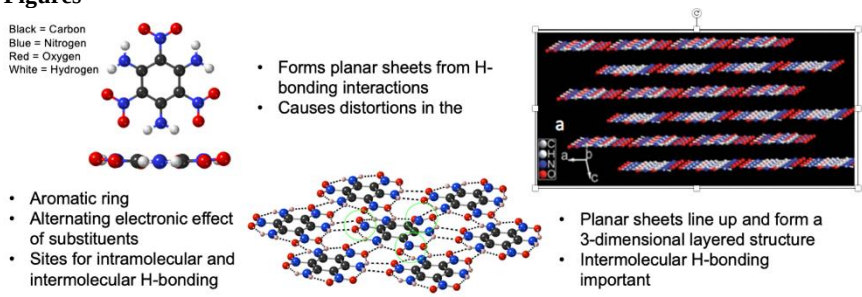

Figure 1 TATB structure: left side—single molecule, middle—single layer array, right side—tertiary layering

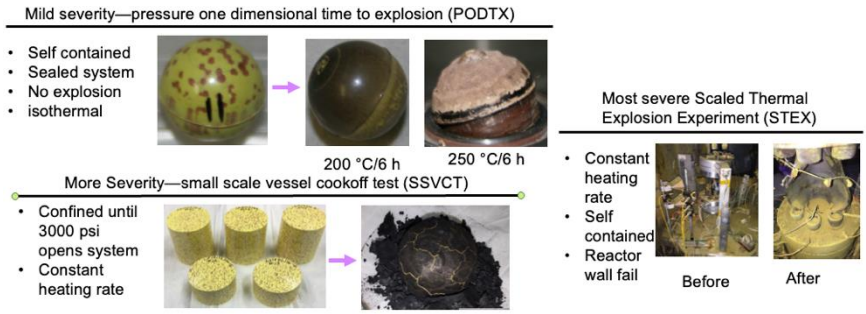

Figure 2 Experimental examples of laboratory configurations for thermal treatment of TATB materials

- Prout-Tompkins[a]
  - $\frac{dX}{dt} = -Ae^{-E/RT}X(1-qX)$
  - $q = 1 - 10^{-p}$
  - 3 parameters
- McGuire & Tarver[b]
  - Solid reactive intermediate
  - 6 parameters
- Tarver et al.[c]
  - Series
  - 6 parameters
- Hobbs & Kaneshige[d]
  - Gas product catalyzed
  - 6 parameters

$$TATB_s \longrightarrow Prod_g$$

$$TATB_s \longrightarrow B_s$$
$$TATB_s + B_s \longrightarrow Prod_g$$
$$2B_s \longrightarrow Prod_g$$

$$TATB_s \longrightarrow B_s \longrightarrow C_s \longrightarrow Prod_g$$

$$0.15\ wt\%\ H_2O_{liq} \rightleftharpoons H_2O_g$$
$$TATB_s \longrightarrow B_s + H_2O_l$$
$$B_s \xrightarrow{P} Prod_g + C_{amorph}$$

a *Trans. Faraday Soc.* **1944**, 488 – 498.
b *7th Symposium on Detonation.* **1981**.
c *J. Phys. Chem.* **1996**, 100, 5794 – 5799.
d *J. Chem. Phys.* **2014**, 140, 124203.

Figure 3 Development of TATB thermal decomposition model from the literature.

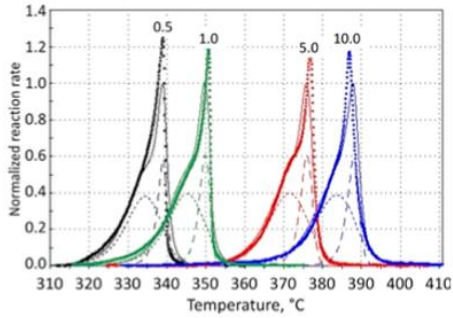

Figure 4 DSC profiles of TATB at of 0.5, 1.0, 5.0, and 120 °C/min heating rates.

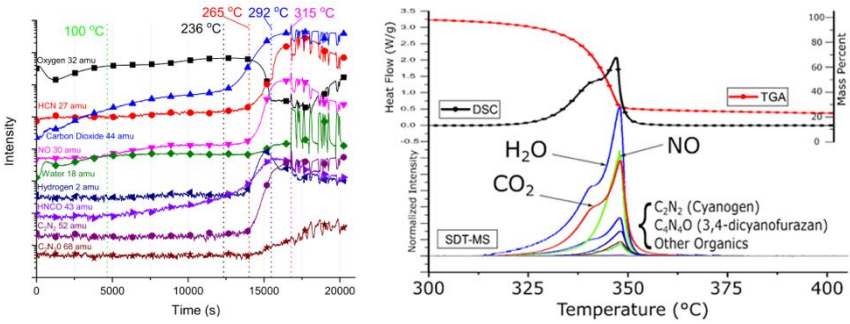

Figure 5. Evolution profiles: left side—masses evolving from monitoring of large-scale cook-off of TATB; right side—heat flow, weight loss and masses evolving from the SDT-MS of TATB at 1 °C/min heating rate.

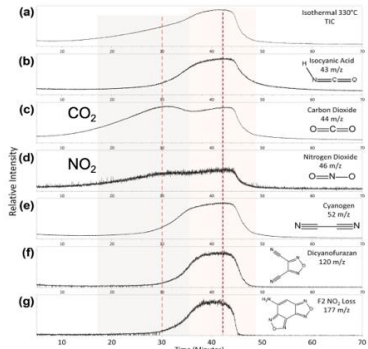

Figure 6. Pyrolysis GC/MS of TATB heated isothermally at 330 °C for 70 min.

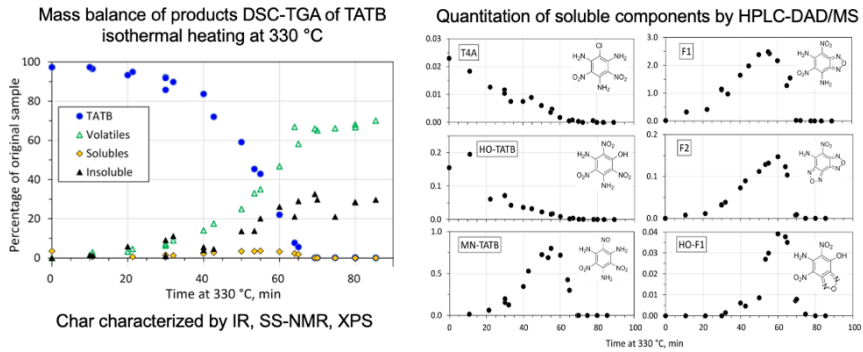

Figure 7. Left side: mass balance of products from the DSC-TGA of TATB heated isothermally at 330 °C for 90 min; right side: selected molecular species identified from products in the DSC-TGA experiments.

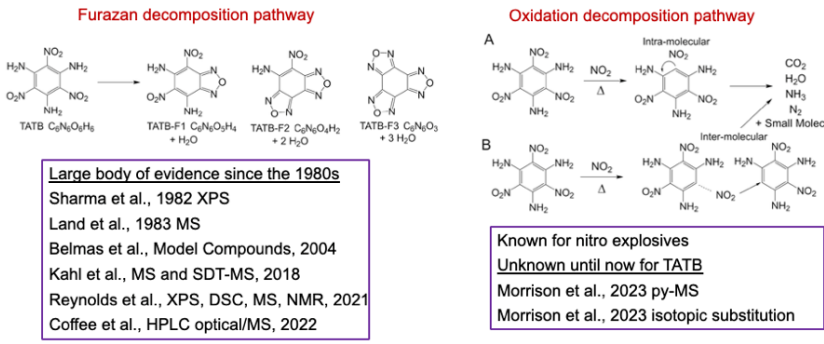

Figure 8. Summary of chemical reaction for the thermal decomposition pathways of TATB

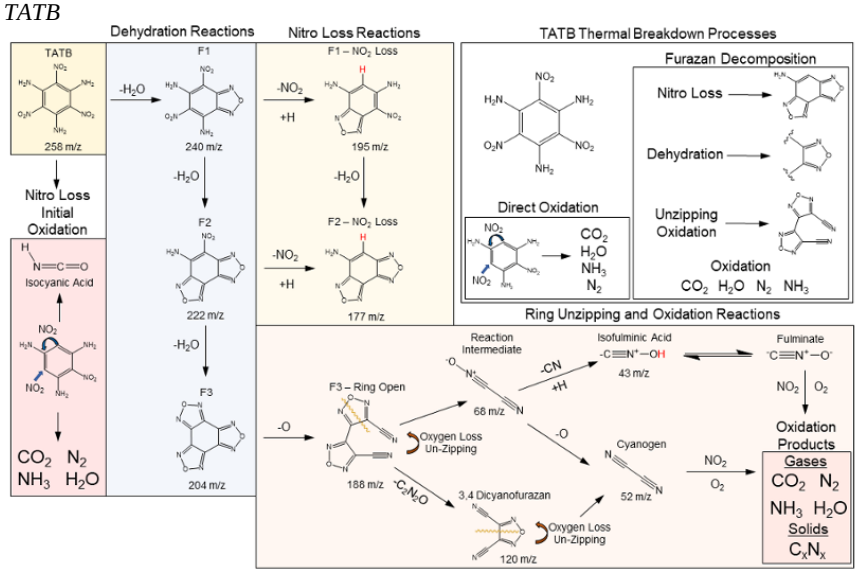

Figure 9. Detailed chemical reaction network for the thermal decomposition pathways of TATB

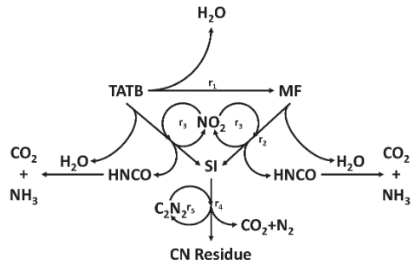

TATB: 1,3,5-triamino-2,4,6-trinitro benzene

MF: mono benzo-furazan

SI: mixture of species from MW 120 (3,4-dicyanofurazan) to 204 (benzo-trifurazan) and higher MW condensed species

CN Residue: mixture of amorphous carbon with nitrogen incorporated structures

Figure 10. Improved thermal decomposition model for TATB.

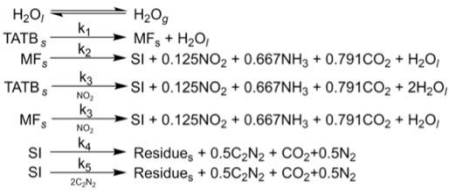

$r_1 = k_{0,1}[TATB]exp(-E_{A,1}/RT)$

$r_2 = k_{0,2}[MF]exp(-E_{A,2}/RT)$

$r_3 = k_{0,3}P[TATB][MF][NO_2]exp(-E_{A,3}/RT)$

$r_4 = k_{0,4}[Solid\ Intermediates]exp(-E_{A,4}/RT)$

$r_5 = k_{0,5}P^2[Solid\ Intermediates]C_2N_2]^2exp(-E_{A,5}/RT)$

Figure 11. Reaction network and rate constants for improved TATB thermal decomposition model

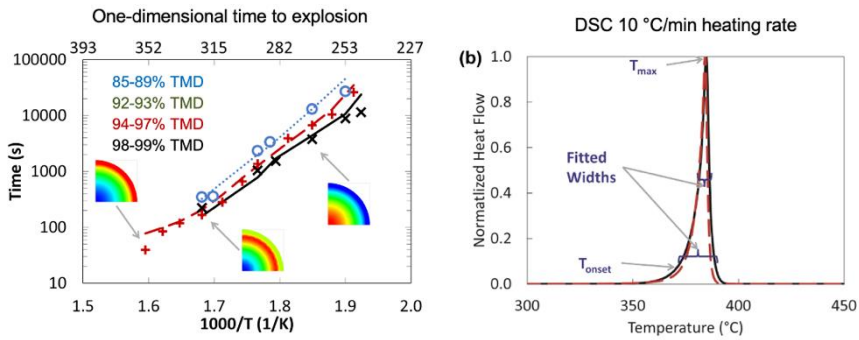

Figure 12. Examples of model simulation compared to experimental data for improved TATB thermal decomposition model.